

IEEE TRANSACTIONS ON CIRCUITS AND SYSTEMS

II: EXPRESS BRIEFS

A PUBLICATION OF THE IEEE CIRCUITS AND SYSTEMS SOCIETY



WWW.IEEE-CAS.ORG

JUNE 2014

VOLUME 61

NUMBER 6

ITCSFK

(ISSN 1549-7747)

Analog and Mixed Mode Circuits and Systems

- An Integrated High-Voltage Low-Distortion Current-Feedback Linear Power Amplifier for Ultrasound Transmitters Using Digital Predistortion and Dynamic Current Biasing Techniques Z. Gao, P. Gui, and R. Jordanger 373
- Charge-Pump Folded Noise Cancellation in Fractional-N Phase-Locked Loops D. Gaied and E. Hegazi 378
- Linearity Enhancement of VCO-Based Quantizers for SD Modulators by Means of a Tracking Loop F. Colodro and A. Torralba 383
- A Genetic Algorithm for the Estimation of Nonidealities in Continuous-Time Sigma-Delta Modulators M. Lorenz, R. Ritter, J. Becker, and M. Ortmanns 388
- K-Band Dual-Mode Receiver CMOS IC for FMCW/UWB Radar G. Pyo, J. Yang, C.-Y. Kim, and S. Hong 393
- A 132-dB Dynamic-Range Global-Shutter Stacked Architecture for High-Performance Imagers A. Khakoni and G. Gielen 398
- Digital Noise-Coupling Technique for Delta-Sigma Modulators With Segmented Quantization L. He, Y. Zhang, F. Long, F. Mei, M. Yu, F. Lin, L. Yao, and X. Jiang 403
- A 100-kS/s 8.3-ENOB 1.7- μ W Time-Domain Analog-to-Digital Converter Y. Kim and C. Yoo 408
- Low-Dropout Voltage Source: An Alternative Approach for Low-Dropout Voltage Regulators H. Aminzadeh, M. R. Nabavi, and W. A. Serdijn 413

Digital Circuits and Systems and VLSI

- Area-Delay-Power Efficient Carry-Select Adder. B. K. Mohanty and S. K. Patel 418
- Low-Power Multicore Processor Design With Reconfigurable Same-Instruction Multiple Process Z. Yu, Z. Yu, X. Yu, N. Liu, and X. Zeng 423
- Linear-Phase VDF Design With Unabridged Bandwidth Control Over the Nyquist Band S. J. Darak, A. P. Vinod, E. M.-K. Lai, J. Palicot, and H. Zhang 428
- Dual-Scan Parallel Flipping Architecture for a Lifting-Based 2-D Discrete Wavelet Transform A. Darji, S. Agrawal, A. Oza, V. Sinha, A. Verma, S. N. Merchant, and A. N. Chandorkar 433
- A 6.4-Gb/s Voltage-Mode Near-Ground Receiver With a One-Tap Data and Edge DFE. S. Kim, E.-Y. Jin, K.-W. Kwon, J. Kim, and J.-H. Chun 438

Circuits and Systems for Communications

- Toward Time-Quantized Pseudorandom Sampling for Green Communication A. Maalej, M. Ben-Romdhane, C. Rebai, A. Ghazel, P. Desgreys, and P. Loumeau 443

Signal Processing

- Efficient Implementation of k -Nearest Neighbor Classifier Using Vote Count Circuit H. Shu, R. Yu, W. Jiang, and W. Yang 448

Control Theory and Systems

- A Novel Stability Analysis for Networked Predictive Control Systems X.-M. Sun, D. Wu, C. Wen, and W. Wang 453
-

Low-Dropout Voltage Source: An Alternative Approach for Low-Dropout Voltage Regulators

Hamed Aminzadeh, *Member, IEEE*, Mohammad R. Nabavi, *Member, IEEE*, and Wouter A. Serdijn, *Fellow, IEEE*

Abstract—In this brief, a high-order temperature-compensated 0.6-V low-dropout voltage source (LDVS) is realized in standard 0.13- μm CMOS technology. The LDVS operates at supply voltages down to 0.75 V and consumes only 39 μA while providing up to 100 mA of load current. Gate-to-channel capacitance values of MOSFETs are employed to implement the capacitors, reducing chip area and enabling integration in any inexpensive CMOS technology. The regulation loop is compensated using a combined pole-splitting and feedforward technique, which results in stable operation from a no-load current to 100 mA of full-load current. A temperature-dependent current-driven voltage generator is proposed to suppress the line-voltage sensitivity of the LDVS. To further improve line regulation, a line-voltage compensation circuit is introduced, which lowers the line sensitivity by about three times down to 0.54%/V. With a supply voltage of 1 V and no output filtering capacitor, the mean power-supply rejection is -51 and -24 dB for 1 and 10 MHz, respectively. The proposed LDVS requires no startup circuit. The 0.1% startup settling time is 73 μs with a supply voltage of 0.8 V and a load current of 1 mA. In the temperature range of -25°C – $+85^\circ\text{C}$, it demonstrates a maximum temperature drift of only 32 ppm/ $^\circ\text{C}$.

Index Terms—Band-gap reference, line-voltage compensation, low-dropout (LDO) regulator, metal-oxide-semiconductor field-effect transistor (MOSFET) only, start up.

I. INTRODUCTION

THE architecture of a typical electronic microsystem consists of several on-chip voltage sources for regulation and comparison [1]. These voltage sources should be independent of the load current I_{Load} , process variation, voltage supply V_{DD} , and temperature. A high-impedance band-gap reference can be designed to be insensitive to temperature. Nonetheless, its high-impedance output node does not remain stable in a harsh and noisy environment. Band-gap references should be followed by a low-dropout regulator (LDO) to drive a load [2]. Conceptually, an LDO amplifies/buffers the output of a band-gap reference within a regulation loop. However, the high-impedance band-gap reference is still vulnerable to transients. Moreover, the reference and LDO should both be optimized for good performance [3].

An alternative is the idea of a low-dropout voltage source (LDVS), depicted in Fig. 1. In this topology, the negative input

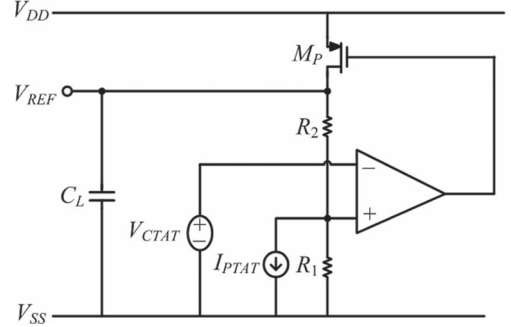


Fig. 1. The proposed LDVS.

terminal of the error amplifier is connected to a complementary-to-absolute-temperature (CTAT) voltage source. In contrast with an LDO, the temperature dependence of the output voltage V_{REF} is directly compensated at the output by adding an extra proportional-to-absolute-temperature (PTAT) current source. Assuming that the dc gain of the amplifier is high, V_{REF} is given by [4]

$$V_{\text{REF}} = (1 + R_2/R_1)V_{\text{CTAT}} + R_2I_{\text{PTAT}}. \quad (1)$$

Therefore, if carefully designed, a buffered yet tunable voltage source (depending on R_2/R_1) is achieved. This configuration has a number of advantages compared to the combination of a reference and an LDO. Foremost, no high-impedance band-gap reference is used in this circuit. High-impedance nodes are vulnerable to load-current transients and also sensitive to supply-coupled noise. Another advantage of the proposed topology is its low temperature drift. For a classical LDO, there is always a residual temperature drift associated with random and systematic offset voltages referred to the output. These types of nonidealities can be considerably compensated for in a circuit that minimizes the errors by means of a negative-feedback control loop.

II. TEMPERATURE COMPENSATION DESIGN CONSIDERATIONS

The temperature drift of V_{REF} in Fig. 1 will be minimized if the temperature behaviors of I_{PTAT} and V_{CTAT} are contrary to each other. The threshold voltages of n-channel MOS (NMOS) and p-channel MOS (PMOS) devices $V_{\text{TH},n}$ and $V_{\text{TH},p}$, respectively, are predominantly CTAT, according to the following [5]:

$$V_{\text{TH}}(T) = V_{\text{TH}}(T_0) - \alpha(T - T_0) \quad (2)$$

where $V_{\text{TH}}(T_0)$ is the threshold voltage at T_0 where α has been evaluated. The thermal voltage $V_T = kT/q$, where k is Boltzmann's constant and q is the electron charge, is, on the other hand, PTAT. Based on these temperature behaviors, the

Manuscript received November 20, 2013; revised January 27, 2014; accepted April 10, 2014. Date of publication April 24, 2014; date of current version June 13, 2014. This brief was recommended by Associate Editor P. Li.

H. Aminzadeh is currently with the Department of Electrical Engineering, Payame Noor University, 19395-4697, Tehran, Iran.

M. R. Nabavi is with Catena Microelectronics, 2628 XG Delft, The Netherlands.

W. A. Serdijn is with the Bioelectronics Section, Delft University of Technology, 2628 CN Delft, The Netherlands.

Color versions of one or more of the figures in this brief are available online at <http://ieeexplore.ieee.org>.

Digital Object Identifier 10.1109/TCSII.2014.2319952

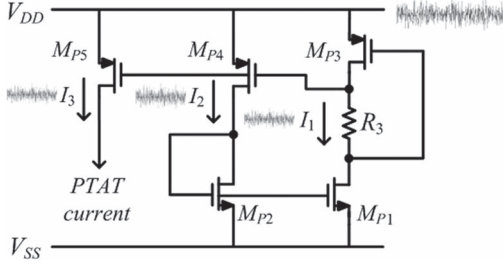


Fig. 2. Schematic of the employed PTAT current generator.

following sub-sections analyze the design considerations that help to minimize the temperature dependence of the proposed LDVS.

A. PTAT Current Generator

The drain current of a PMOS device operating in weak inversion (saturation or triode) is given as

$$I = \left(\frac{W}{L}\right) I_0 \exp\left(\frac{V_{SG}}{NV_T}\right) \left[1 - \exp\left(-\frac{V_{SD}}{V_T}\right)\right] \quad (3)$$

where W/L is the transistor aspect ratio; V_{SG} and V_{SD} are the source–gate and source–drain voltages, respectively; I_0 is a temperature-related parameter of the employed technology; and $N > 1$ is the subthreshold slope factor. Fig. 2 shows a PTAT current generator based on MOS devices operating in the weak-inversion region [6]. In this circuit, the subthreshold devices M_{P3} and M_{P4} generate a PTAT current that is equal to $I_1 = (V_{SG,P3} - V_{SG,P4})/R_3$. Combining this equation and (3) for M_{P3} and M_{P4} , the PTAT current I_1 is related to V_T as

$$I_1 = \frac{NV_T}{R_3} \left\langle \ln \left[\frac{(W/L)_{P1} (W/L)_{P4}}{(W/L)_{P2} (W/L)_{P3}} \right] - \ln \left\{ 1 - \left[\frac{(W/L)_{P4} I_0}{I_2} \right]^N \right\} \right\rangle + \frac{NV_T}{R_3} \ln \left[1 - \exp\left(-\frac{V_{DD} - V_{GS,P2}}{V_T}\right) \right] \quad (4)$$

where $I_2 = (W/L)_{P2}/(W/L)_{P1} \times I_1$. This expression shows that any mismatch between M_{P1} and M_{P2} , or between M_{P3} and M_{P4} , contributes only slightly to the absolute value of I_1 , whereas the nature of the generated current still remains PTAT. The mismatch can be therefore readily compensated by trimming.

As, typically, $V_{DD} - V_{GS,P2} \gg V_T$, $I_2 \gg (W/L)_{P4} I_0$, and $V_{GS,P2} \approx V_{TH,n}$ for small bias currents, I_1 can be approximated as

$$I_1 \approx \frac{NV_T}{R_3} \left\{ \ln \left[\frac{(W/L)_{P1} (W/L)_{P4}}{(W/L)_{P2} (W/L)_{P3}} \right] - \exp\left(\frac{V_{TH,n} - V_{DD}}{V_T}\right) \right\}. \quad (5)$$

The exponential V_{DD} -dependent term in (5) indicates a residual supply dependence in the generated PTAT current I_1 . A solution to this issue is addressed in the following.

B. Line-Voltage Compensation Circuit

Line regulation can be improved by using a line-voltage compensation mechanism for the generated PTAT current. In

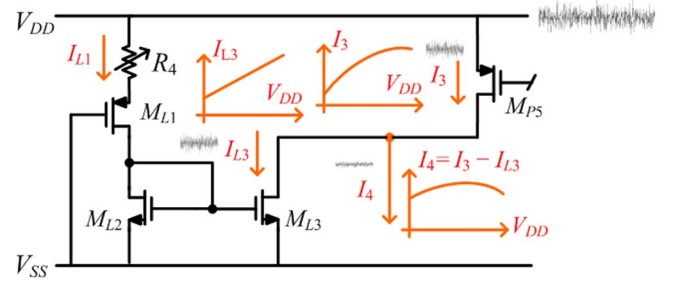
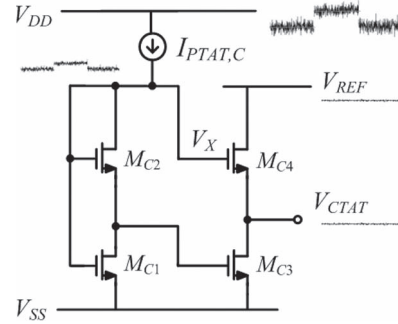
Fig. 3. Proposed line-voltage compensation circuit. (R_4 can be trimmed.)

Fig. 4. Proposed CTAT voltage generator circuit.

Fig. 3, the supply-dependent current I_{L1} is so small that the gate–source voltage of M_{L1} is almost equal to $V_{TH,p}$. Therefore

$$I_{L1} = \frac{V_{DD} - V_{GS,L1}}{R_4} \approx \frac{V_{DD}}{R_4} - \frac{V_{TH,p}}{R_4}. \quad (6)$$

The proposed compensation scheme subtracts a scaled copy of this current I_{L3} from a weighted copy of the original PTAT current I_3 (see Fig. 3). The resulting PTAT current, i.e., $I_4 = I_3 - I_{L3}$, is obtained from

$$I_4 = \frac{NV_T}{R_3} \frac{(W/L)_{P5}}{(W/L)_{P3}} \ln \left[\frac{(W/L)_{P1} (W/L)_{P4}}{(W/L)_{P2} (W/L)_{P3}} \right] + \frac{(W/L)_{L3}}{(W/L)_{L2}} \frac{V_{TH,p}}{R_4} - \frac{NV_T}{R_3} \frac{(W/L)_{P5}}{(W/L)_{P3}} \times \exp\left(\frac{V_{TH,n} - V_{DD}}{V_T}\right) - \frac{(W/L)_{L3}}{(W/L)_{L2}} \frac{V_{DD}}{R_4}. \quad (7)$$

Since the behavior of the last two terms in (7) is contrary to V_{DD} , the supply dependence of I_4 is very limited. This line-voltage compensation mechanism can be practically trimmed over process corners by using R_4 (see Fig. 3). In the fabricated LDVS, the trimming range spans from 100 to 140 k Ω .

C. CTAT Voltage Generator

Fig. 4 depicts the proposed current-driven CTAT circuit as an alternative to a voltage-driven design scheme [7]. Let us suppose that M_{C1} is in strong-inversion triode whereas all the other devices are in strong-inversion saturation. Regardless of the temperature dependence of the biasing current $I_{PTAT,C}$ (i.e., PTAT, CTAT, or constant), the devices can be sized such that the CTAT output V_{CTAT} is merely a function of $V_{TH,n}$. For

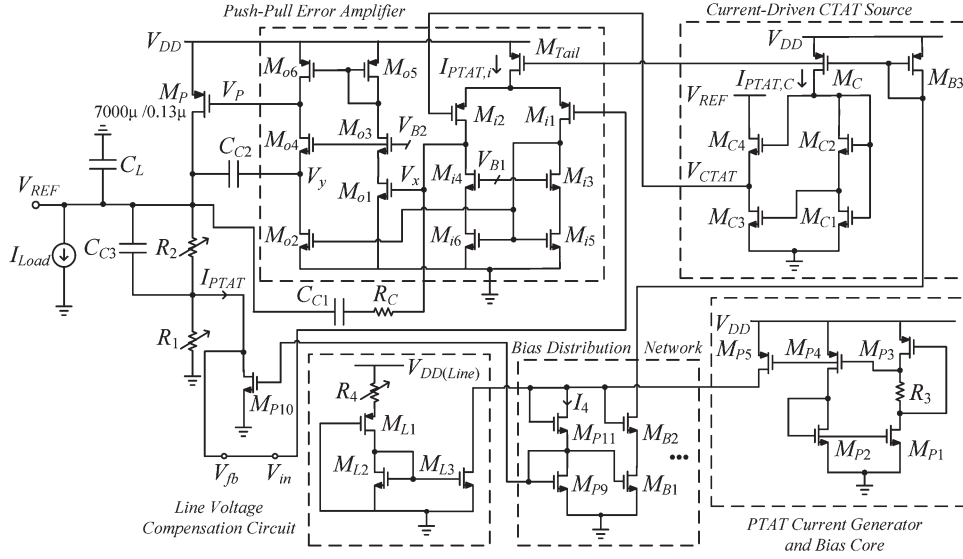


Fig. 5. Proposed voltage source in detail. (R_1 , R_2 , and R_4 can be trimmed to compensate for process variations.)

a PTAT current source as used in this design, the square-law I - V model for the transistors results in

$$V_{CTAT} = \sqrt{\frac{I_{PTAT,C}}{\mu_n C_{ox}}} \times \left[(1 - \sqrt{\gamma}) \sqrt{\frac{1}{(W/L)_{C1}} + \frac{1}{2(W/L)_{C2}}} + (3 + \sqrt{\gamma}) \sqrt{\frac{1}{2(W/L)_{C2}}} \right] + \sqrt{\gamma} V_{TH,n} \quad (8)$$

where $\gamma = (W/L)_{C3}/(W/L)_{C4}$. This expression shows that if

$$\sqrt{\gamma} = \frac{\sqrt{\frac{1}{(W/L)_{C1}} + \frac{1}{2(W/L)_{C2}}} + 3\sqrt{\frac{1}{2(W/L)_{C2}}}}{\sqrt{\frac{1}{(W/L)_{C1}} + \frac{1}{2(W/L)_{C2}}} - \sqrt{\frac{1}{2(W/L)_{C2}}}} \quad (9)$$

the output voltage will be independent of $I_{PTAT,C}$ and can be expressed as

$$V_{CTAT} = \sqrt{\gamma} V_{TH,n}. \quad (10)$$

When using long-channel devices, (8)–(10) describe the CTAT output voltage in a sufficiently accurate manner, at least to the first order. Nonetheless, any residual model error can be readily compensated for by fine-tuning the device sizes during simulations. To satisfy (9), we selected $(W/L)_{C2} = 12(W/L)_{C1}$ and $(W/L)_{C3} = 4(W/L)_{C4}$. Unlike a voltage-driven design scheme [4], [7], the added high-output impedance $I_{PTAT,C}$ shields the sensitive nodes of this circuit from V_{DD} . The supply variations are thus highly attenuated when transferred from V_{DD} to V_{CTAT} . To further protect V_{CTAT} from V_{DD} , the second stage is biased directly from V_{REF} rather than V_{DD} . This therefore results in better line regulation and power-supply rejection. The biasing current of the second stage is defined by the first stage and is not affected by V_{REF} transients. This stable bias current causes V_{CTAT} to be robust against V_{REF} variations.

III. LDVS COMPLETE IMPLEMENTATION

The circuit diagram of the proposed LDVS is shown in Fig. 5 (see also Fig. 1). A two-stage error amplifier with a PTAT tail current ($I_{PTAT,i}$) is employed. The second stage of the

amplifier is push-pull to charge and discharge the gate of the large pass device M_P efficiently. The frequency compensation network consists of C_{C1} , C_{C2} , C_{C3} , and R_C . Capacitor C_{C1} provides pole-splitting at nodes V_X (corresponding to the dominant pole) and V_{REF} (corresponding to a nondominant pole) [8]. The associated right half-plane zero is moved to the left half-plane (LHP) by means of R_C in series with C_{C1} . Capacitor C_{C2} controls the damping factor of the nondominant poles, thereby improving the gain margin [1], [8]. Capacitor C_{C3} generates an LHP zero and adds more phase lead for stable operation. The feedforward stage between V_{in} and V_P (comprised of the input stage and M_{o2} – M_{o4}) operates in parallel with the main stage (comprised of the input stage and M_{o1} – M_{o3} – M_{o5} – M_{o6}). This feedforward stage adds another LHP zero for better stability [8].

The generated I_{PTAT} and V_{CTAT} cancel out each other's temperature dependence, thereby resulting in a temperature-insensitive V_{REF} . By substituting a weighed combination of (7) and (10) into (1) (by considering that $I_{PTAT} = [(W/L)_{P10}/(W/L)_{P9}] \times I_4$) and neglecting the residual supply effect, V_{REF} becomes

$$V_{REF} = \left(1 + \frac{R_2}{R_1}\right) (\sqrt{\gamma} V_{TH,n} + V_{OS}) + \frac{R_2}{R_3} N K_{PTAT} V_T \quad (11)$$

where V_{OS} is the input-referred offset of the error amplifier and

$$K_{PTAT} = \frac{(W/L)_{P10}}{(W/L)_{P9}} \frac{(W/L)_{P5}}{(W/L)_{P3}} \ln \left[\frac{(W/L)_{P1}}{(W/L)_{P2}} \frac{(W/L)_{P4}}{(W/L)_{P3}} \right]. \quad (12)$$

The resistors' ratios R_2/R_1 and R_2/R_3 are temperature independent as they are realized by the same resistor types. Ideally, if V_{OS} is temperature independent, a zero-temperature-coefficient output is achieved for all temperatures when

$$\begin{aligned} \left(1 + \frac{R_2}{R_1}\right) \sqrt{\gamma} \frac{\partial}{\partial T} V_{TH,n} + \frac{R_2}{R_3} N K_{PTAT} \frac{\partial}{\partial T} V_T &= 0 \\ \Rightarrow \frac{R_3}{R_1 \parallel R_2} &= K_{PTAT} \frac{Nk}{q} \frac{1}{\alpha \sqrt{\gamma}}. \end{aligned} \quad (13)$$

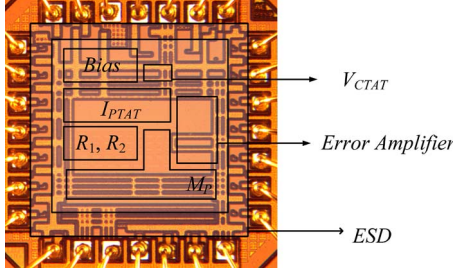


Fig. 6. Chip micrograph.

The resulting V_{REF} is obtained from

$$V_{REF} = \left(1 + \frac{R_2}{R_1}\right) [\sqrt{\gamma} V_{TH,n}(T_0) + \alpha T_0 + V_{OS}]. \quad (14)$$

Equation (14) shows that V_{REF} is ideally a temperature-insensitive voltage reference that can be adjusted by the R_2/R_1 ratio. According to (13), the temperature sensitivity of V_{REF} can be also canceled out by tuning R_3 and/or γ . In practice, however, there are a number of imperfections that cause residual temperature sensitivity. For instance, to derive (14) high-order terms/effects that are temperature dependent such as short channel effects are neglected. Moreover, the addition of the required building blocks (error amplifier, bias network, pass device) adds more temperature drift to the high-order temperature curve achieved.

Measurements confirm that the LDVS in Fig. 5 does not require any dedicated startup circuit. Startup circuits can introduce design difficulties, such as leakage current, and power-up issues during both startup and normal operation [9]. In the proposed LDVS, as soon as the power supply is connected, the PTAT current generation circuit turns on and, in turn, biases all other blocks, which causes the entire LDVS to power up properly.

MOS devices and poly resistors are the only elements used to realize the circuit in Fig. 5. The capacitance values of MOSFETs (MOSCAPs) are area efficient and are compatible with every technology. Unlike the majority of analog circuits, voltage regulators are inherently nonlinear as the location of the poles and zeros depend strongly on the load current. MOSCAP nonlinearity is therefore not detrimental to an already nonlinear LDVS. In this design, C_L , C_{C1} , C_{C2} , and C_{C3} are realized by simple MOS capacitors that help to save area (by about 10% in chip area in this design).

IV. EXPERIMENTAL RESULTS

Fig. 6 depicts a micrograph of the LDVS implemented in IBM's 130-nm CMOS technology. Redundant pins have been assigned to calibrate and test the circuit. The resistors R_1 and R_2 are trimmed (from 630 to 850 k Ω and from 220 to 450 k Ω , respectively) to fine-tune the absolute value of V_{REF} and its temperature drift. This trimming has a negligible impact (e.g., below 1%) on the dynamic characteristics of the LDVS.

Fig. 7 shows the startup settling of V_{CTAT} and V_{REF} for a supply voltage of 0.8 V and a load current of 1 mA. The mean settling time among the tested samples is 73 μ s. By switching on the proposed line-voltage compensation circuit, the no-load line regulation is reduced from +1.4%/V to -0.54%/V (for supply voltages between 0.8 and 1.5 V). The mean power-supply rejection is -51 dB for 1 kHz and -24 dB for 10 MHz, respectively, for a supply voltage of 1 V and a load current of 0 mA.

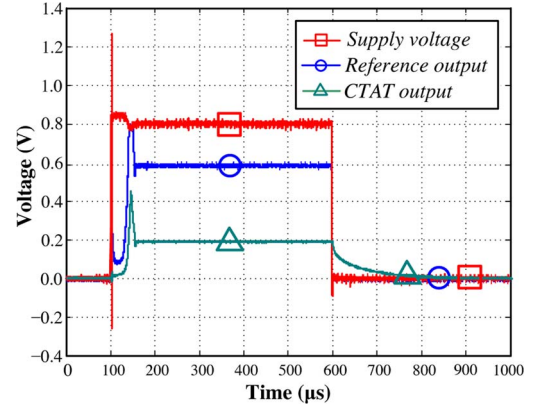
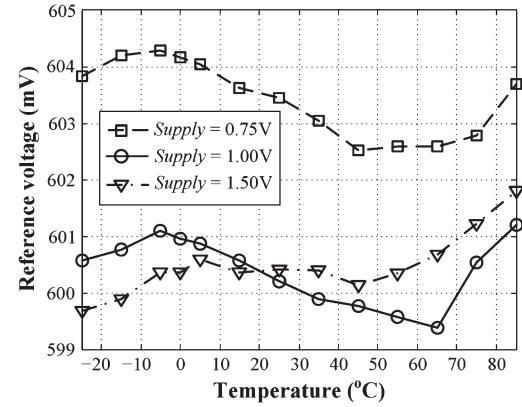
Fig. 7. Measured startup settling response ($V_{DD} = 0.8$ V and $I_{Load} = 1$ mA).

Fig. 8. Measured no-load temperature dependence.

The measured current drawn by the LDVS from a 1-V supply is 39.1 μ A for a load current of 1 mA at a temperature of 25 $^{\circ}$ C. The current reaches 43.2 μ A at 85 $^{\circ}$ C. The error amplifier consumes more than half this current. Without any filtering capacitor, the measured total noise between 0.1 and 10 kHz is 56 μ V for load currents higher than 1 mA. For the same bandwidth, the noise reaches 97 μ V when decreasing the load current to 0 μ A.

Transient load/line responses were tested to verify the performance under various conditions. The load capacitor consists of an integrated MOSCAP (of about 3 pF at $V_{REF} = 0.6$ V) and a parasitic capacitor of about 15 pF. The worst-case 1% settling time of the load response was measured at $V_{DD} = 0.75$ V, when a pulsed load current steps from 0 A to 100 mA and vice versa with a rise/fall time of 0.1 μ s. The settling times are 6.05 and 1.55 μ s, and the overshoot and undershoot are 92 and 270 mV, respectively. The overshoot and undershoot reduce to 73 and 142 mV, respectively, when the rise/fall time is increased to 1 μ s. Increasing the size of the load capacitor also improves the overshoot/undershoot at the cost of more area. For a rise/fall time of 0.1 μ s, the overshoot and undershoot are reduced to 56 and 114 mV, respectively, when using a 100-pF capacitor. The worst-case 1% settling times of the line response are 12.3 and 9.4 μ s, respectively. This is observed at zero-load current when V_{DD} switches from 0.75 to 1.50 V and vice versa with a rise/fall time of 0.2 μ s. For a load current of 100 mA, the 1% settling time reduce to 2.85 and 5.15 μ s, respectively, for a V_{DD} transient with a rise/fall time of 2 μ s. Fig. 8 shows the no-load reference voltage dependence on temperature for different supply voltages. The measured temperature coefficients at 0.75

TABLE I
COMPARISON OF THE PROPOSED WORK WITH PRIOR ART

	This work	Andreou 2012 [10]	Zhan 2012 [11]	Park 2014 [12]	Ng 2011 [3]	Gupta 2007 [2]
Technology	0.13-μm CMOS	0.35- μ m CMOS	0.35- μ m CMOS	0.18- μ m CMOS	0.50- μ m CMOS	0.60- μ m CMOS
Supply range (V)	0.75-1.5	1.7-3.5	1.2	1.8-2.6	0.93-5.0	N/A
Dropout voltage (mV)	148	1100	200	200	702	N/A
Supply current (μ A)	39.14@1.0 V-1 mA 43.20@1.5 V-1 mA	38.35@2.5 V	28@0 μ A	55@1.8 V standby 80@1.8 V operate	28@1.0 V	N/A
Load current range	0-100 mA	0 mA	0-100 mA	0-50 mA	0-9.6 mA	0-5 mA
Temp. compensation type, value (ppm/ $^{\circ}$ C)	High-order 26@0.75 V-0 μA 32@1.50 V-0 μA	High-order 3.9 [-15 $^{\circ}$ C, 150 $^{\circ}$ C] 13.7 [-50 $^{\circ}$ C, 150 $^{\circ}$ C]	N/A	N/A	First-order 34 [-20 $^{\circ}$ C, 120 $^{\circ}$ C]	First-order 34.7 [N/A]
Line regulation (%/V)	-0.54@0 μA -0.57@100 mA	0.039	0.39@100 mA	N/A	3.68	N/A
Power-supply rejection (dB)	-51@1 kHz -24@10 MHz	N/A	-49.8@1 kHz -13@1 MHz	-70@1 MHz -37@10 MHz	-58@100 Hz -12@1 MHz	-30.8@500 kHz -8.1@4 MHz
Tran. load settling time (μ s)	6.05/1.55	N/A	\sim 5	<10	<10	N/A
step size - rise/fall time	100 mA - 0.1 μs	N/A	100 mA - 1 μ s	50 mA - 0.1 μ s	0.35 mA	5 mA - 0.1 μ s
overshoot/undershoot (mV)	92/270@20 pF	N/A	50/105@100 pF	120/80@100 pF	>100 mV@100 pF	U.S. > 500 mV
Active area (mm ²)	0.31*	0.102	0.0987	0.14**	0.0464	N/A

* Including the additional circuitry for trimming, measurement and test purposes.

** Excluding on-chip capacitor.

and 1.5 V are 26 and 32 ppm/ $^{\circ}$ C, respectively, when the temperature changes from -25 $^{\circ}$ C to +85 $^{\circ}$ C. A comparison between this paper and a number of recently reported band-gap references and voltage regulators [2], [3], [10]–[12] is presented in Table I. The transient load regulation is comparable with the LDOs reported in [2], [3], [11], and [12] when considering the value of the load capacitor, the step size, the rise/fall time of I_{Load} and, finally, the overshoot/undershoot and the settling time of the output. The temperature coefficient is higher than the specifications reported in [10]. However, the proposed voltage source is designed to source up to 100 mA for supply voltages down to 0.75 V. The voltage reference in [10] has a minimum supply voltage of 1.7 V with a dropout voltage as large as 1.1 V. It cannot provide any load current either. Compared with [11], the proposed LDVS achieves a higher order temperature curve at a considerably lower supply voltage. The main advantages of the proposed low-voltage voltage source are high-order temperature response, high-current drive capability, and minimum dropout voltage. These advantages, however, result in an increase in the area compared with the architectures in Table I. One reason for this increase is the use of relatively large devices required to cope with the smaller voltage headroom at lower supply voltage. This, in turn, leads to the need for the multipath compensation network that also calls for more area. By using the proposed line-voltage compensation technique, the line sensitivity of the proposed LDVS is comparable with that of the stand-alone LDOs with the benefit of high-order temperature compensation.

V. CONCLUSION

The design and analysis of a high-order buffered LDVS have been presented in this brief. Measurement data of a 100 mA–600 mV voltage source show that the circuit can achieve a temperature coefficient of up to 32 ppm/ $^{\circ}$ C. Temperature compensation is achieved by properly combining the outputs of a PTAT current generator with a proposed current-driven CTAT voltage

generator in a closed-loop configuration. A line-voltage compensation technique reduces the line sensitivity by a factor of three.

REFERENCES

- [1] K. N. Leung and P. K. T. Mok, "A capacitor-free CMOS low-dropout regulator with damping-factor-control frequency compensation," *IEEE J. Solid-State Circuits*, vol. 38, no. 10, pp. 1691–1702, Oct. 2003.
- [2] V. Gupta and G. A. Rincon Mora, "Low-output impedance 0.6 μ m CMOS sub-bandgap reference," *IET Electron. Lett.*, vol. 43, no. 20, pp. 1085–1086, Sep. 2007.
- [3] D. C. W. Ng, D. K. K. Kwong, and N. Wong, "A sub-1 V, 26 μ W low-output-impedance CMOS bandgap reference with a low dropout or source follower mode," *IEEE Trans. Very Large Scale Integr. (VLSI) Syst.*, vol. 19, no. 7, pp. 1305–1309, Jul. 2011.
- [4] H. Aminzadeh, R. Lotfi, and K. Mafinezhad, "Low-dropout voltage reference: An approach to low-temperature-sensitivity architectures with high drive capability," *IET Electron. Lett.*, vol. 45, no. 24, pp. 1200–1201, Nov. 2009.
- [5] I. M. Filanovsky and A. Allam, "Mutual compensation of mobility and threshold voltage temperature effects with application in CMOS circuits," *IEEE Trans. Circuits Syst. I, Reg. Papers*, vol. 48, no. 7, pp. 876–883, Jul. 2001.
- [6] M. H. Cheng and Z. W. Wu, "Low-power low-voltage reference using peaking current mirror circuit," *IET Electron. Lett.*, vol. 41, no. 10, pp. 572–573, May 2005.
- [7] L. Toledo, C. Dualibe, P. Petrashin, and W. Lancioni, "A novel supply-independent biasing scheme for use in CMOS voltage reference," in *Proc. Conf. DCIS*, 2005.
- [8] K. N. Leung and P. K. T. Mok, "Analysis of multistage amplifier frequency compensation," *IEEE Trans. Circuits Syst. I, Reg. Papers*, vol. 48, no. 9, pp. 1041–1056, Sep. 2001.
- [9] A. Boni, "Op-amps and startup circuits for CMOS bandgap references with near 1-V supply," *IEEE J. Solid-State Circuits*, vol. 37, no. 10, pp. 1339–1343, Oct. 2002.
- [10] C. M. Andreou, S. Koudounas, and J. Georgiou, "A novel wide-temperature-range, 3.9 ppm/ $^{\circ}$ C CMOS bandgap reference circuit," *IEEE J. Solid-State Circuits*, vol. 47, no. 2, pp. 574–581, Feb. 2012.
- [11] C. Zhan and W.-H. Ki, "An output-capacitor-free adaptively biased low-dropout regulator with subthreshold undershoot-reduction for SoC," *IEEE Trans. Circuits Syst. I, Reg. Papers*, vol. 59, no. 5, pp. 1119–1131, May 2012.
- [12] C.-J. Park, M. Onabajo, and J. Silva-Martinez, "External capacitor-less low drop-out regulator with 25 dB superior power supply rejection in the 0.4–4 MHz range," *IEEE J. Solid-State Circuits*, vol. 49, no. 2, pp. 486–501, Feb. 2014.

BROWSE ▾

MY SETTINGS ▾

MY PROJECTS

WHAT CAN I ACCESS?

RESOURCES ▾

SEARCH

[beta](#)
[Author Search](#) | [Advanced Search](#) | [Preferences](#) | [Search Tips](#) | [More Search Options ▾](#)[Browse Journals & Magazines](#) > [Circuits and Systems II: Express Briefs, IEEE](#) ...

Circuits and Systems II: Express Briefs, IEEE Transactions on

 Add Journal To My Alerts View Title History

Popular

Early Access

Current Issue

Past Issues

About Journal

Submit Your Manuscript

Popular Articles (July 2014)

Includes the top 25 most frequently downloaded documents for this publication according to the most recent monthly usage statistics.

☐ Select All Results Download Citations Save to Project Email Selected Results Print**1. Area-Delay-Power Efficient Carry-Select Adder**

Mohanty, B.K. ; Patel, S.K.

 PDF (727 KB)**2. Efficient FPGA and ASIC Realizations of a DA-Based Reconfigurable FIR Digital Filter**

Sang Yoon Park ; Meher, P.K.

 PDF (675 KB)**3. An Integrated High-Voltage Low-Distortion Current-Feedback Linear Power Amplifier for Ultrasound Transmitters Using Digital Predistortion and Dynamic Current Biasing Techniques**

Zheng Gao ; Ping Gui ; Jordanger, R.

 PDF (583 KB)**4. Low-Dropout Voltage Source: An Alternative Approach for Low-Dropout Voltage Regulators**

Aminzadeh, H. ; Nabavi, M.R. ; Serdijn, W.A.

 PDF (708 KB)**5. An Energy-Efficient Low Frequency-Dependence Switching Technique for SAR ADCs**

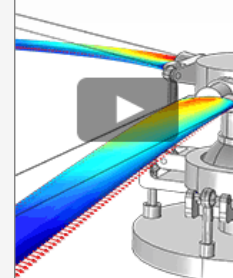
Sanyal, A. ; Nan Sun

 PDF (532 KB)**6. Charge-Pump Folded Noise Cancellation in Fractional-N Phase-Locked Loops**

Gaied, D. ; Hegazi, E.

 PDF (894 KB)

What Is
Multiphysics
Simulation?

[LEARN MORE](#) COMSOL